21

Interferometry in Wireless Sensor Networks

Sandor Szilvasi[1], Peter Volgyesi[1], Janos Sallai[1],
Akos Ledeczi[1] and Miklos Maroti[2]
[1]*Institute for Software Integrated Systems, Vanderbilt University*
[2]*Bolyai Institute, University of Szeged*
[1]*USA*
[2]*Hungary*

1. Introduction

Wireless Sensor Networks (WSN) consist of small, low-cost, resource-constrained embedded computers equipped with low-power radios and various sensors. When deployed, they form an ad-hoc wireless network and sense the environment cooperatively. Application areas of WSNs include environmental monitoring, healthcare, structural monitoring and the military among others. Many WSN applications rely on the location of sensor nodes in order to make consistent spatio-temporal observations. Sensor node localization, therefore, has been an active research area for the past decade.

Consequently, a wide variety of localization methods has been proposed for WSNs. Among the most popular are acoustic and radio signal-based approaches. The limited range of acoustic methods make them impractical for anything but small scale deployments. The best known radio-based method is the Global Positioning System (GPS). For outdoor applications that require absolute localization accuracy in the order of meters, GPS is generally a good solution. However, its price and power requirement restrict its applicability to high-end WSNs. In indoor and urban environments, heavily affected by multipath effects, Ultra Wide band (UWB) methods offer high accuracy by measuring the Time of Flight (TOF) or Time Difference of Arrival (TDOA) of a short pulse-waveform to deduce ranges Tuchler et al. (2005), Fontana et al. (2003). The UWB-based techniques typically achieve sub-meter ranging error where the accuracy depends mainly on the available bandwidth, which in turn is constrained by emission regulations. UWB has not become popular in WSNs primarily due to its high cost.

Techniques based on received radio signal strength (RSS) gained significant popularity in WSNs as they require no specialized hardware; they use the radio chip readily available on WSN nodes. RSS-based ranging measurements are also simple as they typically consist of averaging the value of the radio chip RSS signal. The operating range is limited to the communication range of the radio with a precision of a few meters Taubenheim et al. (2005).

This research was partially supported by ARO MURI grant W911NF-06-1-0076 and the TÁMOP-4.2.2/08/1/2008-0008 program of the Hungarian National Development Agency.

However, the measurement is highly environment dependent. Achieving reasonable accuracy requires extensive calibration prior to ranging. Uncalibrated RSS ranging can exhibit 10-20% errors.

A novel ranging method based on radio interferometry (RI) for static WSN node localization was introduced in Maróti et al. (2005). This RI ranging method measures the phase of the radio signals to obtain information on the relative distance between the sensor nodes. It achieves sub-meter localization accuracy and long range simultaneously. As this RI approach also relies solely on the radio chip readily available on popular, low-cost commercial off-the-shelf (COTS) sensor nodes, it became an alternative to RSS-based methods and, thus, garnered considerable attention in the WSN community. Since its original debut, improvements in several directions have been proposed. Dil & Havinga (2011) drops the requirement that a low frequency interference signal need to be synthesized through tuning and copes with the problem taking a stochastic approach. Contrary, Amundson et al. (2010) assumes a priori knowledge of certain node locations and transforms the range estimation into a bearing estimation problem. RI phase measurement based techniques generally outperform other currently available methods that use no specialized hardware, such as RSS-based methods. However, they also require more sophisticated ranging measurements and computationally more intensive fusion of the ranging data as shown in Figure 1. Furthermore, as multipath propagation heavily impacts the phase measurement accuracy, their performance degrades significantly in indoor environments.

	Signal strength based	**Signal phase based**
Accuracy	Low (beyond a few meters)	High (up to hundreds of meters)
Ranging measurement complexity	Very low	High
Localization complexity	Low, trilateration	High
Additional hardware required	No	No
Bandwidth requirement	Low	Medium

Table 1. Comparison of received signal strength (RSS) and signal phase based localization

While the above techniques measure either the signal strength or phase, radio-interferomentric methods exploiting the Doppler effect deduce information from the signal frequency. The measured frequency change of the radio signal produced by a moving transmitter is a function of its velocity relative to the receiver. In a WSN with a few static nodes with known locations, this relative velocity can be used to track mobile transmitters Kusý et al. (2007). Inverting the roles, the Doppler-shift technique is used for localization Lédeczi et al. (2008): the technique replaces the static receivers with rotating transmitters around a known point with a known angular speed. The receiver nodes, in turn, can calculate their bearings from these anchors. RI is applied in both cases to allow precise measurement of the frequency change on resource constrained WSN nodes. Unfortunately, these methods still suffer from the adverse effect of multipath propagation. Furthermore, the rotation of the receivers calls for special hardware, usually unavailable on WSN nodes.

This chapter describes the baseline approach of radio interferometry based localization and details the many developments that occurred since its introduction. Section 2 lays down the

mathematical foundation of the localization method, which is then referenced throughout the rest of the chapter. It also presents the first platform using this approach, called the Radio Interferometric Positioning System (RIPS), along with a discussion of the initial results. Section 3 introduces a method for tracking mobile nodes in WSNs utilizing the phenomena of Doppler effects and radio interferometry. The technique shown in Section 4 exploits the Doppler effect in a different way to determine the location of static nodes in a WSN. It relies on a few distinct nodes with known locations (anchors) to first calculate the bearing to the rest of the nodes and to deduce location information based on the bearing estimates. The technique presented in Section 5 also calculates bearings from anchor nodes, but instead of using Doppler shifts, it uses a special arrangement of RIPS which allows for an enhanced, distributed method of node localization.

2. Radio interferometric positioning

The basic idea behind interferometric localization is to use the phase information of a radio signal to measure distance. In practice, however, this is hard to achieve, because it would require (a) nanosecond-precision timing, (b) precise control over the phase of the transmitted signal, and (c) precise phase detection on the receiver. COTS radio transceivers commonly used in sensor nodes do not offer these features. The novelty of the method presented in this chapter is to use a transmitter pair and a receiver pair to eliminate the unknown initial phase of the respective local oscillators (LO), as well well as to allow for a low-speed ADC to process the incoming signal on the receiver.

The interferometric approach thus utilizes a pair of wireless sensor nodes to generate interfering radio signals by transmitting pure sinusoids at slightly different frequencies. The envelope of this composite signal has a beat frequency equal to the frequency difference of the sinusoids, as illustrated in Figure 2. It is the phase of the envelope signal that is of most interest, as it carries location related information. When measured at two receivers at the same time, the instantaneous phase difference (also referred to as the *phase offset*) of the respective interference signal envelopes is directly related to the carrier wavelength and the relative distance between the transmitters and receivers. Working with the envelope signal instead of the "raw" carrier signal has several advantages. On one hand, the envelope frequency depends on only the frequency difference of the transmitted sinusoids. This means that the received envelope frequency is the same at all receivers, and it is independent of the frequency and initial phase of the receivers' local oscillators. On the other hand, the envelope frequency can be precisely controlled (in short term), thus it is adjustable to meet the available time synchronization accuracy, limited sampling rate and processing capability of the wireless sensor nodes.

The rest of the section discusses the theory of radio interferometric localization in detail.

2.1 Idealistic phase-based localization

Let us consider, hypothetically, that the transmitted signal's phase is controllable, and the received phase can be detected accurately.

These sinusoids we refer to as carrier signals, though they are not modulated.

Here, the measured phase at the receiver as a function of the distance from the receiver is

$$\varphi = 2\pi \left(\frac{d}{\lambda} \right) \mod (2\pi), \tag{1}$$

where φ_i is the measured phase, d is the receiver's distance from the transmitter and $\lambda_i = c/f$ is the wavelength of the RF signal. A representative received phase map is is shown in Figure 1.

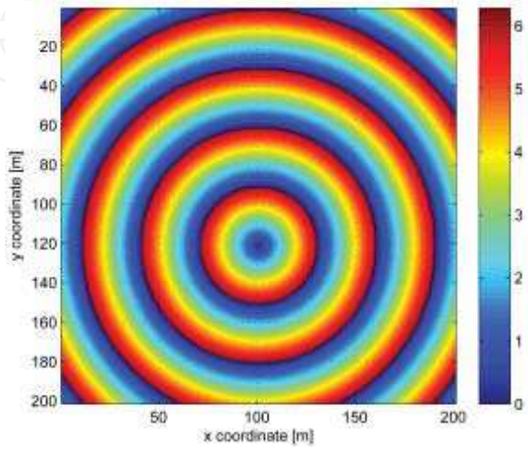

Fig. 1. Phase map of an unmodulated carrier signals assuming controllable transmitter phase and accurate phase detection at the receiver.

From here, we can express the distance as follows.

$$d_i = \frac{\varphi_i}{2\pi}\lambda_i + k \cdot \lambda_i \qquad k \in \mathbb{Z} \tag{2}$$

This means that the receiver is capable of measuring its distance from the transmitter with a mod (λ_i) ambiguity. By repeating the measurement at different wavelengths, it is possible to determine the unambiguous distance from the transmitter within the effective radio range of the transmitter, thereby restricting the possible receiver positions to a single circle around the receiver. Then, this is repeated for several other transmitters to gain multiple circles intersecting at a single point, at the position of the receiver.

2.2 Interferometric localization

In WSNs, however, the nodes have independent LOs and neither their initial phase, nor their relative phase to each other can be assumed to be known. Maróti et al. (2005) suggests the use of transmitter and receiver pairs along with radio interferometry to deduct location information from the phase of propagating radio waves without assumptions on the LO initial phases.

2.2.1 Phase measurement

A ranging measurement starts with two transmitters emitting high-frequency pure sinusoid radio signals with slightly different frequencies f_1 and f_2. Due to variations of the LO crystals,

precise tuning of the frequency difference $f_1 - f_2$ is required, which is achieved through a *calibration* process. Once the calibration is done, the received composite signal at a receiver node, see Figure 2, takes the following form:

$$s(t) = a_1 \cos(2\pi f_1 t + \varphi_1) + a_2 \cos(2\pi f_2 t + \varphi_2). \tag{3}$$

Interestingly, the envelope of $s(t)$ preserves important phase information such as the $\varphi_1 - \varphi_2$

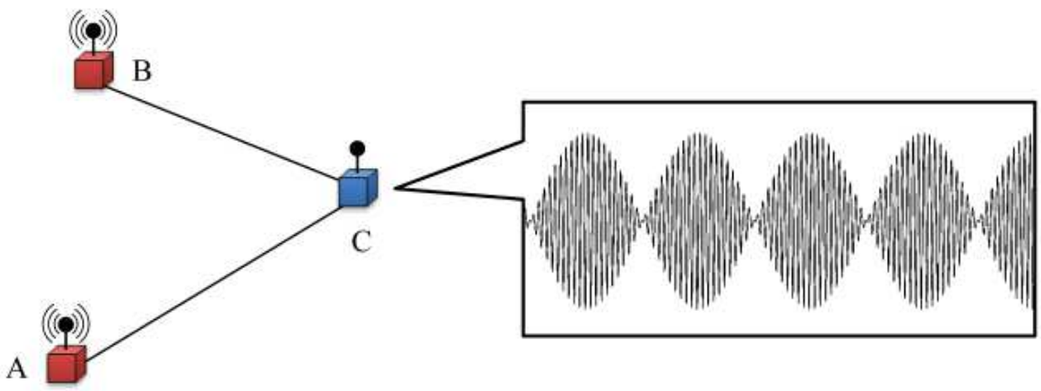

Fig. 2. The radio interferometric signal generated by two independent transmitters received by a third node

phase offset the two carriers. To show this, let the carrier signal be down-mixed to the intermediate frequency f_{IF}. Denoting the mean of the two transmitted frequencies (f_1 and f_2) with $\delta = (f_1 - f_2)/2$ and assuming $f_2 < f_1$, $\delta \ll f_2$ and that the down-mixing introduces zero phase shift, the intermediate frequency signal can be written as

$$s_{\text{IF}}(t) = a_1 \cos\big(2\pi(f_{\text{IF}} + \delta)t + \varphi_1\big) + a_2 \cos\big(2\pi(f_{\text{IF}} - \delta)t + \varphi_2\big). \tag{4}$$

The envelope of this signal is accessed by first calculating its power:

$$\begin{aligned} s_{\text{IF}}^2(t) = {} & a_1^2 \cos^2\big(2\pi(f_{\text{IF}} + \delta)t + \varphi_1\big) + a_2^2 \cos^2\big(2\pi(f_{\text{IF}} - \delta)t + \varphi_2\big) \\ & + 2a_1 a_2 \cos\big(2\pi(f_{\text{IF}} + \delta)t + \varphi_1\big) \cos\big(2\pi(f_{\text{IF}} - \delta)t + \varphi_2\big). \end{aligned} \tag{5}$$

Applying the following trigonometric identities

$$\cos^2(x) = \frac{1}{2} + \frac{\cos(2x)}{2} \tag{6}$$

$$\cos(x)\cos(y) = \frac{\cos(x+y)}{2} + \frac{\cos(x-y)}{2}, \tag{7}$$

the square of $s_{\text{IF}}(t)$ can be rewritten as

$$\begin{aligned} s_{\text{IF}}^2(t) = {} & \frac{1}{2}(a_1^2 + a_2^2) + \frac{a_1^2}{2} \cos\big(4\pi(f_{\text{IF}} + \delta)t + 2\varphi_1\big) + \frac{a_2^2}{2} \cos\big(4\pi(f_{\text{IF}} - \delta)t + 2\varphi_2\big) \\ & + a_1 a_2 \cos\big(4\pi f_{\text{IF}} t + \varphi_1 + \varphi_2\big) + a_1 a_2 \cos\big(4\pi\delta t + \varphi_1 - \varphi_2\big), \end{aligned} \tag{8}$$

where the components are either at zero frequency (DC), $2(f_{\mathrm{IF}} \pm \delta)$, $2f_{\mathrm{IF}}$ or 2δ. Removing the DC, and the $2f_{\mathrm{IF}} \pm \delta$ and $2f_{\mathrm{IF}}$ double-IF frequency components by appropriate filtering we obtain the envelope signal

$$r(t) = a_1 a_2 \cos\left(2\pi(2\delta)t + \varphi_1 - \varphi_2\right), \tag{9}$$

where the frequency of $r(t)$ is $2\delta = f_1 - f_2$ and the $\varphi_1 - \varphi_2$ phase corresponds to the phase offset of the two carrier signals. That is, by measuring the phase of the the envelope signal, $r(t)$, the phase difference of the two carriers can be obtained *independently of the receiver LO initial phase*.

2.2.2 Q-range estimation

The carrier phase offset in the form of Equation 9 is unsuitable to deduct location information directly. Interstingly, however, when it is measured at two different nodes in a time synchronized manner, it allows to gain information on the relative distances between the transmitters and receivers.

To show this, consider Figure 3, where transmitters A and B generate the interfering carrier signals and receivers C and D extract the envelope signals $r_C(t)$ and $r_D(t)$, respectively.

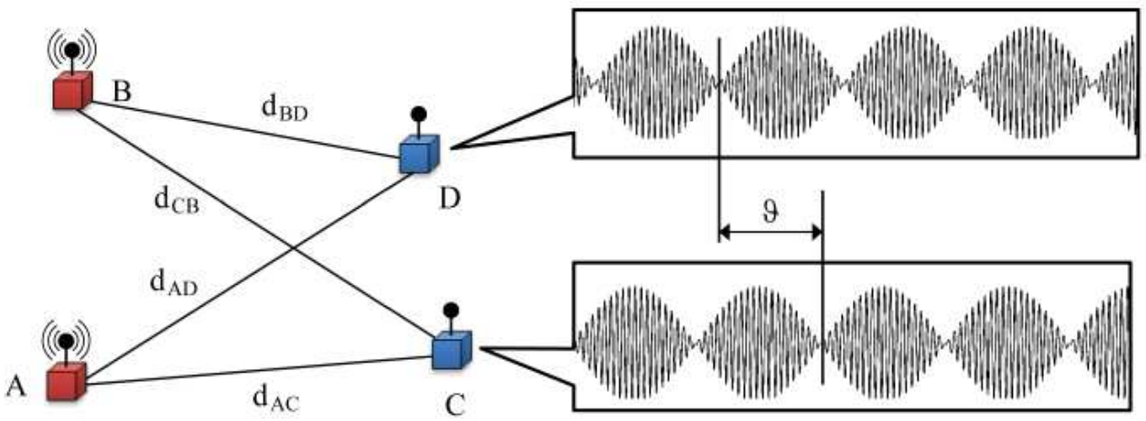

Fig. 3. Radio interferometric ranging performed by a pair of transmitters and a pair of receivers.

Let Y be a receiver node, and let A and B be the two transmitters. Let t_A and t_B be the time when node A and B start to transmit, respectively. Furthermore, let a_{AY} and a_{BY} the amplitude of the attenuated signal as received at node Y from node A and B, respectively. The received composite signal at node Y is

$$\begin{aligned} s_Y(t) &= a_{AY} \cos\left(2\pi f_A (t - t_A - d_{AY}/c)\right) \\ &\quad + a_{BY} \cos\left(2\pi f_B (t - t_B - d_{BY}/c)\right) \\ &= a_{AY} \cos\left(2\pi f_A t - 2\pi f_A (t_A + d_{AY}/c)\right) \\ &\quad + a_{BY} \cos\left(2\pi f_B t - 2\pi f_B (t_B + d_{BY}/c)\right) \end{aligned} \tag{10}$$

after sufficient amount of time, that is when t is greater than $t_A + d_{AY}/c$ and $t_B + d_{BY}/c$. Using Equation 9, the absolute phase offset of the envelope signal $r_Y(t)$ is

$$\vartheta_Y = -2\pi f_A(t_A + d_{AY}/c) + 2\pi f_B(t_B + d_{BY}/c). \tag{11}$$

Now consider the two receivers C and D. The relative phase offset of $r_C(t)$ and $r_D(t)$ is

$$\begin{aligned}\vartheta_C - \vartheta_D &= -2\pi f_A(t_A + d_{AC}/c) + 2\pi f_B(t_B + d_{BC}/c) \\ &\quad + 2\pi f_A(t_A + d_{AD}/c) - 2\pi f_B(t_B + d_{BD}/c) \\ &= 2\pi f_A/c \cdot (d_{AD} - d_{AC}) + 2\pi f_B/c \cdot (d_{BC} - d_{BD}).\end{aligned} \tag{12}$$

From this the relative phase offset of $r_C(t)$ and $r_D(t)$ is

$$2\pi\Big(\frac{d_{AD} - d_{AC}}{c/f_A} + \frac{d_{BC} - d_{BD}}{c/f_B}\Big) \pmod{2\pi}. \tag{13}$$

Due to the limited range of wireless sensor nodes and their high carrier frequency relative to the envelope frequency, the above formula of the measured relative phase offset can be simplified. Consider Figure 3 again, where nodes A and B transmit pure sine waves at two close frequencies $f_A > f_B$, and two other nodes C and D measure the envelope of the signal. Using the notation $\delta = (f_A - f_B)/2$, the relative phase offset of $r_C(t)$ and $r_D(t)$ is

$$\vartheta_C - \vartheta_D = 2\pi\frac{d_{AD} - d_{AC} + d_{BC} - d_{BD}}{c/f} + 2\pi\frac{d_{AD} - d_{AC} - d_{BC} + d_{BD}}{c/\delta} \pmod{2\pi}.$$

Assuming that $f_A - f_B < 2$ kHz and $d_{AC}, d_{AD}, d_{BC}, d_{BD} \leq 1$ km, it follows that $c/\delta \geq 300$ km and thus the second term can be neglected. Now, if for any four nodes A, B, C and D we define a quantity called the *q-range* as

$$d_{ABCD} = d_{AD} - d_{BD} + d_{BC} - d_{AC}, \tag{14}$$

then for any frequency f the relative phase offset simplifies to

$$\vartheta_{ABCD} = 2\pi\frac{d_{ABCD}}{c/f} \pmod{2\pi}. \tag{15}$$

Thus, if adequately precise time synchronization is available, the receiver can effectively measure ϑ_{ABCD} and calculate d_{ABCD} with a $\lambda = c/f$ wave length ambiguity.

Similarly to Figure 1, the phase ambiguity corresponds to equi-phase-offset curves (or surfaces in three dimension) in Figure 4. Note, that while Figure 1 plots the phase of the signal transmitted by a single transmitter, Figure 4 depicts the phase offset of the interference signal transmitted by a transmitter pair relative to that of a reference receiver. That is, the equi-phase-offset curves with respect to a reference receiver are multiple hyperbolas in Figure 4. If the phase offset measurement is repeated at i different carrier wavelengths λ_i for the same set of nodes A, B, C and D, we get the following set of equations by reorganizing Equation 15:

$$d_{ABCD} = \frac{\vartheta_{ABCD}}{2\pi}\lambda + k\lambda \quad (k \in \mathbb{I}) \tag{16}$$

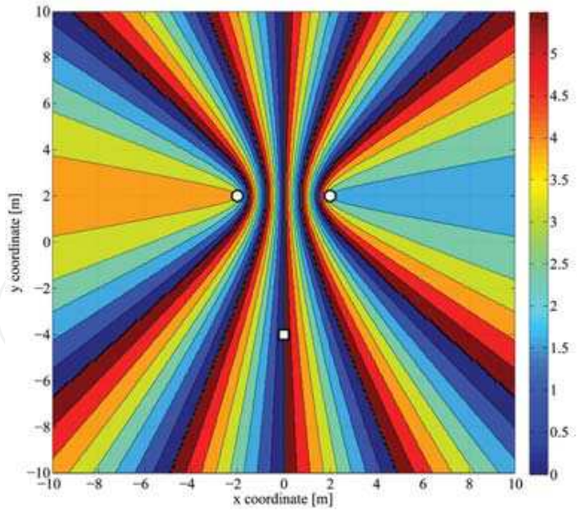

Fig. 4. Map of phase difference with respect to a reference receiver at (0,-4), when the interference signal is created by two independent transmitters located at (-2,0) and (2,0), respectively.

To compute the q-range estimate d_{ABCD}, we have to solve not only for d_{ABCD}, but also for integers k_i. Clearly, no closed form solution exists, given the integer ambiguity in the equations. However, direct search techniques are possible, since in practice the q-range is constrained by the effective radio communications range, thereby restricting the search space. In practice, the measured q-range is always between $-2r$ and $2r$, r being the radio's maximum transmission distance. Kusý et al. (2006) describe a search heuristic that finds the q-range by minimizing the error of the q-range estimate with respect to the available phase offset measurements:

$$\hat{d}_{ABCD} = \underset{\hat{d}_{ABCD} \in [-2r, 2r]}{\arg\min} \sum_{i=1}^{N} \left| \frac{\varphi_i}{2\pi} \lambda_i + k_i \lambda_i - \hat{d}_{ABCD} \right| \tag{17}$$

2.2.3 Position estimation

Once the necessary amount of q-ranges is obtained from the radio-interferometric phase measurements, the position of the individual nodes is determined by finding the optimum of a set of constrained non-linear equations. For this optimization problem Maróti et al. (2005) suggests to use least-squares (LS) error fitting of the j q-range measurements:

$$(\hat{x}, \hat{y}) = \underset{\hat{x}, \hat{y}}{\arg\min} \sum_{j=1}^{M} (d_{ABCD,j} - \hat{d}_{ABCD,j})^2. \tag{18}$$

Maróti et al. (2005) describe a genetic search algorithm to localize the network. Dil & Havinga (2011) observed that LS approach is highly suspectible to outliers, and propose to use the Least Absolute Deviation (LAD) instead:

$$(\hat{x}, \hat{y}) = \underset{\hat{x}, \hat{y}}{\arg\min} \sum_{j=1}^{M} |d_{ABCD,j} - \hat{d}_{ABCD,j}|. \tag{19}$$

2.3 Platform description and results

The first interferometry based localization system, the Radio Interferometric Localization System, was presented in Maróti et al. (2005). The RIPS uses the popular MICA2 wireless sensor nodes equipped with CC1000 radio chip Texas Instruments (2007a). The fine grained LO tuning capability of the CC1000 allows to precisely set the interference frequency to 300-700 Hz in the 433 MHz band. On the downside, the sampling rate of the interference signal is limited to 9 kHz by the ADC found on the MICA2.

Nonetheless, this relatively low sampling rate proves to be sufficient for accurate phase offset measurements when accompanied with precise, microsecond order time synchronization among the independent sensor nodes. In RIPS, two transmitter nodes generate the interference signal and the receiver nodes measure its envelope phase in a time-synchronized manner, at particular time instant. This is repeated on 11 different radio channels in the 400 MHz to 430 MHz range. The measured phase values are sent to a PC using WSN communication infrastructure. (Notice that the CC1000 radio chip is used for both localization and communication.) For a given pair of transmitters, the PC calculates the phase offsets of all possible pairs of receivers. As the number of participating recivers, and thus the phase measurements, is limited only by the communication range, the PC calculates the q-ranges for the same transmitter pair and all possible combination of the receivers with valid phase measurements. The whole process is then repeated with different combination of transmitters to acquire a large number of q-ranges. The q-ranges are then used as input for a genetic algorithm (GA) to optimize the heavily non-linear localization problem expressed by Equation 18. The output of the GA is the relative coordinates of the sensor nodes, assuming no a priori knowledge on any of the node locations.

The 16-node experiment on a 18×18 m outdoors area showed that RIPS was able to localize the nodes with an average error less than 5 cm. For that, 240 different transmitter combinations were used and the overall localization process took approximately 80 minutes.

3. Doppler shift-based tracking

Tracking of mobile sensor nodes in a WSN has been another active area of research in the past years. It is typically more challenging that localizing static nodes as the latency needs to be low enough to keep up with the mobility. On the other hand, estimating the current location of a node is aided by the already obtained estimate of the previous location. Similarly to static localization, a number of different methods have been proposed in the literature. When the most natural solution, GPS is not available due to cost or power constraints, interferometry offers an alternative.

The original idea of the Doppler shift-based tracking presented in Kusý et al. (2007) assumes a set of stationary infrastructure nodes, *anchor nodes*, and another set of *mobile nodes* that need to be tracked – both with known locations initially. The tracking system aims for power-efficiency by remaining inactive as long as the tracked nodes stay still. Tracked nodes are responsible for maintaining their location, detecting their movement and invoking the tracking service only when movement is detected. Once a tracked node reports movement, the tracking system becomes active and assists the mobile node to determine its location and velocity.

On the fundamental level, the provided tracking service is based on the phenomenon of Doppler effect or Doppler shift. The movement of a radio signal transmitter relative to a stationary receiver introduces a change in the observed signal frequency as illustrated in Figure 5.

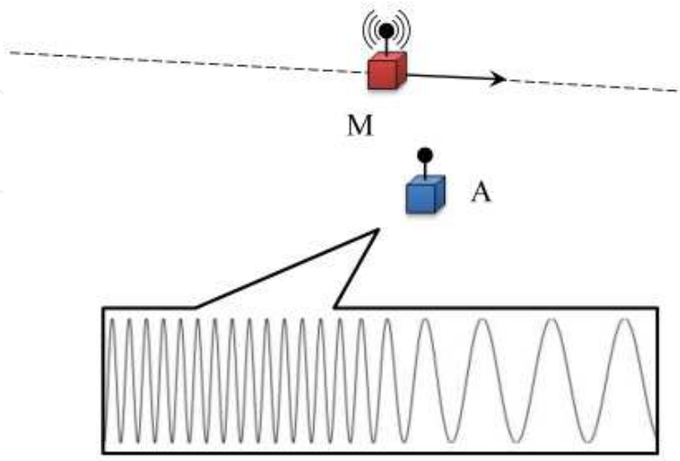

Fig. 5. Illustration of the Doppler frequency shift in the signal introduced by the relative velocity of the moving transmitter to the stationary receiver.

The velocity of the mobile transmitter is directly related to the change in the received signal frequency, thus, by precisely measuring the frequency deviation, the velocity can be estimated. In order to improve measurement accuracy by canceling the receiver side LO uncertainty, an interference signal similar to the one introduced in Section 2 is utilized. When the tracking service is invoked, the mobile node and *one* anchor node transmit their unmodulated carrier at close frequencies. The rest of the anchor nodes measure the frequency change in the interference signal envelope and report the estimates to a central unit. The central unit fuses frequency change information to calculate the location and velocity of the mobile node simultaneously. The derived location and velocity estimates are then fed to a Kalman filter to keep the state information of the nodes up-to-date.

The remainder of the section starts by detailing the interferometry based Doppler shift measurement. That is followed by the description of the location and velocity estimation formulated as a non-linear optimization problem, and the Kalman filter used for tracking. Finally, a prototype implementation on the CC1000 radio chip based MICA2 platform is shown.

3.1 Interferometric tracking

Radio interferometric tracking based on doppler shifts is naturally divided into the *measurement* of doppler shifts and *tracking* phases, that is, the fusion of the doppler shift measurements. Throughout the discussion, nodes are classified either as *anchor nodes* with known positions, or as *mobile nodes* that need to be localized. The interferometry based Doppler shift measurement utilizes an interference signal similar to the one described in Section 2. However, while interferometric ranging estimates the phase of the interference signal, interferometric tracking exploits the frequency shift of the same signal induced by

the movement of a transmitting mobile node. The radio interferometric Doppler shift measurement begins with an anchor node and the mobile node to be localized transmitting pure sinusoid waveforms at slightly different frequencies. Consider Figure 6, where A denotes an anchor node and M the mobile node, both acting as transmitters, and the rest as receiver anchor nodes. Let M and A transmit an unmodulated carrier with frequencies f_M, and F_A respectively, such that $f_M > f_A$. The two carriers interfere with each other and create a signal with an envelope frequency of $f_M - f_A$. This interference signal is measured by a number of anchor nodes A_i. As M moves among the anchor nodes A_i, they observe f_M to be Doppler shifted by Δf_M^i, where the value of Δf_M^i depends on the relative speed of M to A_i.

Transmitter A is stationary and its singal is not affected by the doppler shift, thus the measured envelope frequency at receiver node A_i becomes

$$f_i = f_M - f_A + \Delta f_M^i. \tag{20}$$

This allows for the calculation of the Doppler shift measured at node A_i and, consequently, the relative speed of the tracked node.

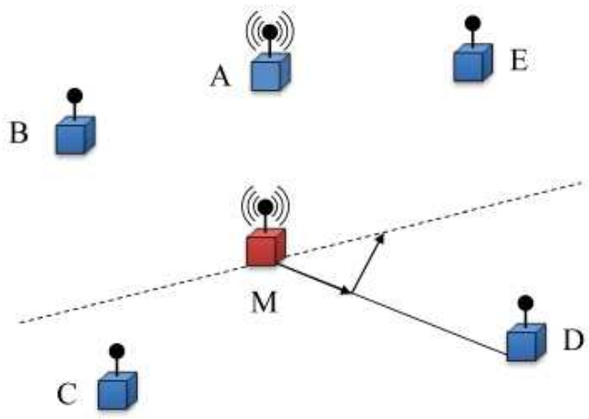

Fig. 6. Doppler shift-based tracking of a mobile node (M) using several stationary nodes (A-E).

Let $\vec{v}$ denote the velocity of the tracked mobile node M and $\vec{u}_i = \overrightarrow{A_iM}/\|A_iM\|$ the unit length vector pointing from anchor node A_i to M. The relative speed of A_i and M can then be defined as the following dot product

$$v_i = \vec{u}_i \cdot \vec{v}, \tag{21}$$

where v_i is a scalar value with positive sign if $\vec{v}$ points away from A_i and negative sign otherwise.

The Doppler equation states that if f is the frequency of the transmitted radio signal, c is the speed of light, and $v \ll c$ is the speed of the source with respect to the observer (with negative sign of v if the source was going towards the observer), then the observed frequency is $f' = (1 - v/c)f$. Therefore,

$$\Delta f = f' - f = -vf/c. \tag{22}$$

Using $\widehat{f} = f_M - f_A$ and $\lambda_M = c/f_M$, the node A_i observes the interference signal with frequency

$$f_i = \widehat{f} - v_i/\lambda_M \tag{23}$$

which can be measured at node A_i. Consequently, if the $\widehat{f}$ difference of the two transmitted frequencies is known, the relative speed of the tracked node M and the anchor node A_i can be calculated.

Note that estimating the frequency difference $\widehat{f}$ with sufficient accuracy becomes a problem when using low-cost radio transceivers due to LO inaccuracies. The use of radio interferometry instead of direct carrier signals partially alleviates this issue by removing the receiver side LO uncertainty. However, as the transmitter side LO may still drift, $\widehat{f}$ is treated as an unknown parameter in the tracking phase.

In the tracking phase the Doppler shifts measured by multiple infrastructure nodes are utilized to calculate the location and the velocity of a tracked node. The tracking problem is modeled as a non-linear optimization problem where the location coordinates (x, y) and the velocity vector $\vec{v} = (v_x, v_y)$ of the tracked node need to be determined. Due to the uncertainty in the transmitted signal frequencies f_M and f_A, the interference frequency $\widehat{f} = f_M - f_A$ is also treated as a parameter to be estimated. Consequently, the full parameter vector $\mathbf{x}$ of the optimization problem is

$$\mathbf{x} = (x, y, v_x, v_y, \widehat{f})^\top. \tag{24}$$

Assuming that n anchor nodes measure the Doppler shifted radio signal, there are n frequency observations f_i. Therefore, the observation vector $\mathbf{c}$ is defined as

$$\mathbf{c} = (f_1, f_2, \ldots, f_n)^\top. \tag{25}$$

The relation of the parameter vector $\mathbf{x}$ and the observation vector $\mathbf{c}$ can be formalized as a function $H : \mathcal{R}^5 \to \mathcal{R}^n$, such that

$$\mathbf{c} = H(\mathbf{x}). \tag{26}$$

The function H is a vector-vector function consisting of n functions $H_i : \mathcal{R}^5 \to \mathcal{R}$, each of them calculating the Doppler shifted interference frequency f_i measured at an infrastructure node A_i. From Equation 23, $H_i(\mathbf{x})$ is defined as

$$H_i(\mathbf{x}) = \widehat{f} - v_i/\lambda_M. \tag{27}$$

The relative speed v_i of the mobile node M to an anchor node A_i can be calculated from the location of the two nodes and the velocity $\vec{v}$ of the tracked node M, as shown in Figure 7. Using the distributive property of the dot product and the identities $\vec{v} = \vec{v}_x + \vec{v}_y$ and $|\vec{u}_i| = 1$ the relative velocity becomes

$$v_i = \vec{u}_i \cdot \vec{v} = \vec{u}_i \cdot \vec{v}_x + \vec{u}_i \cdot \vec{v}_y = |\vec{v}_x| \cos\alpha + |\vec{v}_y| \sin\alpha, \tag{28}$$

where $\sin\alpha$ and $\cos\alpha$ can be calculated from coordinates (x, y) and (x_i, y_i) of nodes M and A_i, respectively. This allows for the calculation of the expected measurements $f_i = H_i(\mathbf{x})$ from

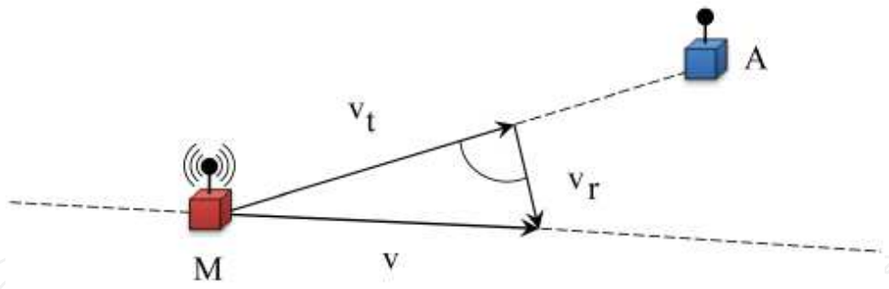

Fig. 7. Vector decomposition of the mobile node velocity $\vec{v} = \vec{v}_t + \vec{v}_r$ as observed by the receiver anchor node A.

the parameter vector $\mathbf{x}$ and the known quantities λ_M, x_i, y_i:

$$H_i(\mathbf{x}) = \widehat{f} - \frac{1}{\lambda_M} \frac{v_x(x_i - x) + v_y(y_i - y)}{\sqrt{(x_i - x)^2 + (y_i - y)^2}} \tag{29}$$

As due to measurement errors, there may exist no $\mathbf{x}$ such that $H(\mathbf{x}) = \mathbf{c}$, the parameters are estimated by finding $\mathbf{x} \in \mathcal{R}^5$ such that $\|H(\mathbf{x}) - \mathbf{c}\|$ is minimized. Note that components of the objective function H are non-linear functions, requiring the use of non-linear optimization methods.

3.2 Platform description and results

The Doppler shift-based tracking uses radio interferometry to enable frequency shift measurements on resource constrained WSN platforms, such as the CC1000 equipped MICA2. The latter platform is capable of synthesizing a 300-700 Hz interference frequency in the 433 MHz band on the transmitter side, and to accurately measure frequency shifts in the envelope of the interference signal despite its limited, 9 kHz, sampling rate. Therefore, identical sensor nodes can be used both as anchor nodes and as mobile nodes.

Kusý et al. (2007) suggests to find the initial locations at deployment time with an accurate and possibly computationally more expensive algorithm, such Maróti et al. (2005), and switch to Doppler shift-based tracking afterwards. Once the initial positions are available, the tracking system starts in listening mode and operates on a per-request basis. A mobile target node can invoke the tracking service of the anchor nodes by sending a request message and starting to transmit an unmodulated carrier signal. In response, one of the anchor nodes start transmitting at a close frequency, while the rest measure frequency changes in the interference signal caused by the movement of the mobile node. The relative speed is calculated from the frequency shift by Equation 23 at every anchor node, which is then fed into an extended Kalman filter (EKF) running on a PC to keep an up-to-date model of the node location.

Measurements with eight anchor nodes and a single mobile node in a 50×30 m field indicated that the Doppler shift-based tracking of a mobile node with a speed between 1 and 3 m/s can be performed with an average location error of 1.5 m, speed error of 0.14 m/s and heading error of 7.2°. The update interval of the EKF is the sum of the 0.3 s coordination phase, 0.4 s measurement time and 1.0 s to route the measurement results to the PC, resulting in 1.7 s latency.

4. Doppler shift-based localization

The methods presented in Section 2 and Section 3 for localization and tracking both have the adventage that they use WSN nodes equipped with the same hardware throughout the entire system. The distinction between any two nodes is their actual role (e.g. *transmitter/receiver, mobile/anchor*) and the a priori knowledge of their location. Also, both methods call for computationally expensive non-linear optimization at the sensor fusion phase. However, by specializing certain nodes in the system the "workload" of the fusion phase can be significantly decreased.

Lédeczi et al. (2008) and Chang et al. (2008) proposed the idea to use physically *rotating anchor* nodes in WSNs for node self-localization. Their underlying approach is similar to the one used for mobile node tracking, described in Section 3, in many aspects. Anchor nodes represent key elements of the localization service and measurements rely on the Doppler effect, which in turn utilize radio interferometry. However, the Doppler effect is used in a different way. Instead of having the tracked node and an anchor node transmitting the interfering carrier signals it is two anchor nodes that transmit. One of the anchor nodes is equipped with no specialized hardware, while the other one has a "spinning" antenna. This spinning either refers to the physical rotation of a single antenna or its imitation using an antenna array. In both cases, the target nodes observe a Doppler shift in the received signal due to the actual or virtual rotational movement of the transmitter antenna. The measured Doppler shift is used by the target nodes to determine their bearing from the anchor nodes. The bearing estimates from multiple anchor node pairs are then used to determine the actual location of the target node.

The remainder of this section details the theory behind the Doppler-shift based localization methods using rotating-antenna and antenna-array anchor nodes, their first WSN implementation, and experimental results.

4.1 Bearing estimation with rotating-antenna anchor nodes

The Doppler shift-based radio interferometric localization with rotating-antenna anchor nodes is divided into two distinct phases, *bearing estimation* and *localization*. In the bearing estimation phase, the nodes to be localized, the *target nodes*, measure the Doppler shift in the carrier signal introduced by the rotational movement of the anchor node antenna and deduct bearing information. The localization phase takes the bearing estimates and the anchor node locations to determine the target node location via triangulation.

The bearing estimation starts with two anchor nodes, a rotating and a fixed one, transmitting unmodulated sinusoid carriers at close frequencies, where the fixed node can be an arbitrarily selected transmitter node with known location. Receiver nodes extract the envelope of the interference signal, see Equation 9, and measure its frequency.

Note that radio interferometry is utilized to make frequency estimation feasible on resource constrained sensor nodes as any frequency change in the envelope signal equals to that of the original carrier. Thus, assuming the additional transmitter node has ideal accuracy, its presence and the details of radio interferometry will be temporarily ignored in the following discussion.

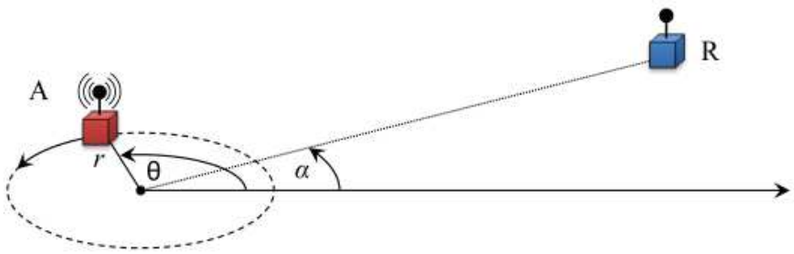

Fig. 8. Doppler shift generated by the rotating-antenna anchor node.

The measured frequency change is related to the movement of the transmitter through the Doppler effect, $\Delta f = vf/c$, where v is the tangential component of the transmitter velocity relative to the receiver, f is the carrier frequency and c is the speed of light. To discuss the case where the transmitter antenna is rotating, consider Figure 8. The antenna of the anchor node, A_{rot}, is rotating counterclockwise around the origin with a radius r and a constant angular velocity ω. Let $\vec{v}(t)$ denote the velocity of the rotating antenna A_{rot} and $\vec{u}_r = \overrightarrow{RA}_{rot}/\|RA_{rot}\|$ the unit length vector pointing from the receiver node R to A_{rot}. The relative speed of A_{rot} and R can then be defined as the following dot product

$$v_p(t) = \vec{u}_r \cdot \vec{v}(t), \tag{30}$$

where

$$\vec{v}(t) = \left(-\omega r \sin(\omega t + \varphi), \omega r \cos(\omega t + \varphi)\right). \tag{31}$$

Therefore, the receiver node R observes the projected velocity component $v_p(t)$:

$$v_p(t) = \vec{u}_r \cdot \vec{v}(t) = \frac{-\omega r d \sin(\omega t + \varphi)}{\sqrt{d^2 + r^2 - 2dr\cos(\omega t + \varphi)}} \tag{32}$$

Consequently, the observed frequency change at R is

$$\begin{aligned} \Delta f = \frac{v_p(t)}{c} f &= \frac{f}{c} \frac{-\omega r d \sin(\omega t + \varphi)}{\sqrt{d^2 + r^2 - 2dr\cos(\omega t + \varphi - \alpha)}} \\ &= \frac{-\omega r f}{c} \frac{\sin(\omega t + \varphi - \alpha)}{\sqrt{1 + (r/d)^2 - 2(r/d)\cos(\omega t + \varphi - \alpha)}}. \end{aligned} \tag{33}$$

Assuming that the rotational radius is significantly smaller than the node distance, $r \ll d$, the expression of Δf simplifies to

$$\lim_{r/d \to 0} \Delta f = \frac{-\omega r f}{c} \sin(\omega t + \varphi). \tag{34}$$

The argument of the expression in Equation 34 then becomes

$$\omega t + \varphi - \alpha = \sin^{-1}\left(\frac{-c\Delta f}{\omega r f}\right). \tag{35}$$

Thus, instead of estimating the φ initial phase of the rotating anchor, a second receiver, a *reference* node can be used to eliminate the $(\omega t + \varphi)$ term. Let R_2 denote the reference node as

in Figure 9. The α angle between the two nodes is obtained by subtracting the two arguments:

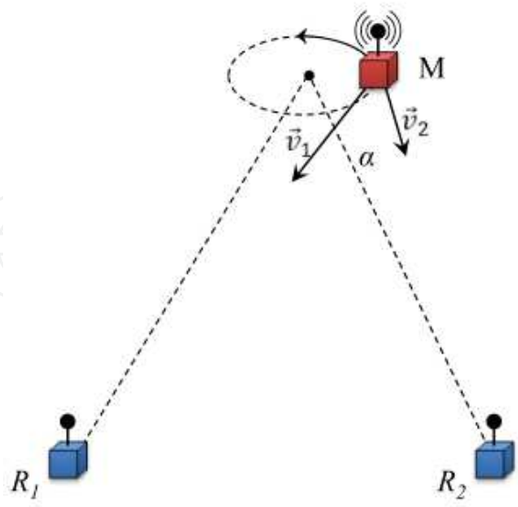

Fig. 9. Estimation of the angle between two receivers and a rotating anchor node.

$$\alpha = \sin^{-1}\left(\frac{c\Delta f_{R_1}}{\omega r f}\right) - \sin^{-1}\left(\frac{c\Delta f_{R_2}}{\omega r f}\right) \tag{36}$$

4.2 Bearing estimation with antenna-array anchor nodes

Similarly to the rotating-antenna case, bearing estimation starts with two anchor nodes transmitting unmodulated sinusoids at close frequencies to construct the interference signal. One of these anchor nodes is equipped with multiple circularly arranged antennas, while the other one can be any node of the WSN with a priori known location. The antenna array mimics the physical rotation of a single antenna by switching between the antennas in sequence - enabling only one at a time. The receivers process the envelope of the interference signal to obtain bearing information through the quasi Doppler shift caused by the imitated movement of the antenna. Note, that in case of ideal transmitters, any change in the carrier frequency introduces the same amount of frequency shift in the detected envelope signal. Therefore, the presence of the interferometry is temporarily disregarded in the following discussion, despite its heavy use in real WSN measurements. Consider an N element uniform circular array (UCA) as depicted in Figure 10. The virtual rotation of the antenna over the N locations results in a constant frequency signal with sudden phase jumps. As a corner case, when $N \to \infty$ the magnitude of phase changes converge to the Doppler shift frequency, essentially giving the same results as the physically rotating antenna discussed in Section 4.1. Thus, by measuring the N discrete phase changes over a full turn of the virtual antenna, the frequency of the mimicked rotating antenna can be calculated at N different locations along the UCA. Assume that the radius of an N-element UCA is negligible compared to receiver to transmitter distance and let the angular speed of the virtually rotating antenna be ω. The phase change between time instants t and Δt then becomes:

$$\Delta\phi(t, t+\Delta t) = \frac{\int_t^{t+\Delta t} sin(\omega t)dt}{\Delta t} = sin\left(\omega t + \frac{\Delta t}{2}\right)\frac{2sin(\frac{\Delta t}{2})}{\omega\Delta t}, \tag{37}$$

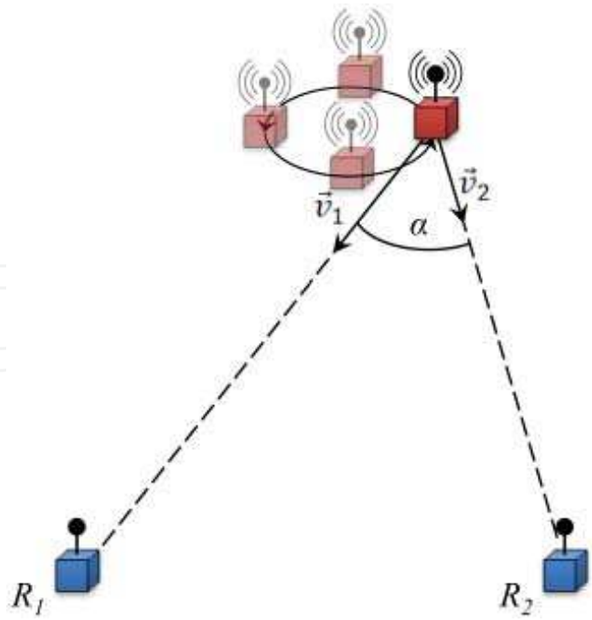

Fig. 10. Quasi doppler bearing estimation using only four discrete (N=4) steps instead of continuous rotation.

where $\omega = 1/(N\Delta t)$. Thus, by measuring the N phase jumps throughout a full turn of the antenna, the $\sin(\omega t + \varphi)$ term can be estimated. The phase of this signal is then used to calculate the bearing to the anchor nodes in a similar fashion as described in Section 4.1.

4.3 Localizaton based on bearing estimates

The localization phase takes multiple angle estimates, α_i, between the target node, rotating-antenna or antenna-array node i and the reference node, as depicted in Figure 11, and deduces the location of node Q. In the optimal case, the bearing estimates intersect at a single point. Due to measurement errors, however, bearing estimates $\alpha_i (i > 2)$ to target node Q may have multiple intersections. In this case, an optimization algorithm can be used to estimate the most probable target node location.

4.4 Platform description and results

The Doppler shift-based SpinLoc localization system presented in Chang et al. (2008) uses MICA2 type CC1000 equipped sensor nodes both for anchor nodes and target nodes, where the rotating-antenna transmitter anchors are physically rotated on a 50 cm radius arm, at 133 revolutions per minute (RPM) by a servo motor. The measurements use the 900 MHz band to generate the 600 Hz interference signal and measure its frequency change.

The measurement round starts with time synchronization initiated by the base station. The rotating anchor node and a static node starts transmitting the unmodulated carriers, which is received and processed by a reference node and the target nodes. The latter two calculate the signal frequencies and send it to the base station. A PC attached to the base station then calculates the orientation of the rotating anchors, the relative bearings and the position of the target nodes.

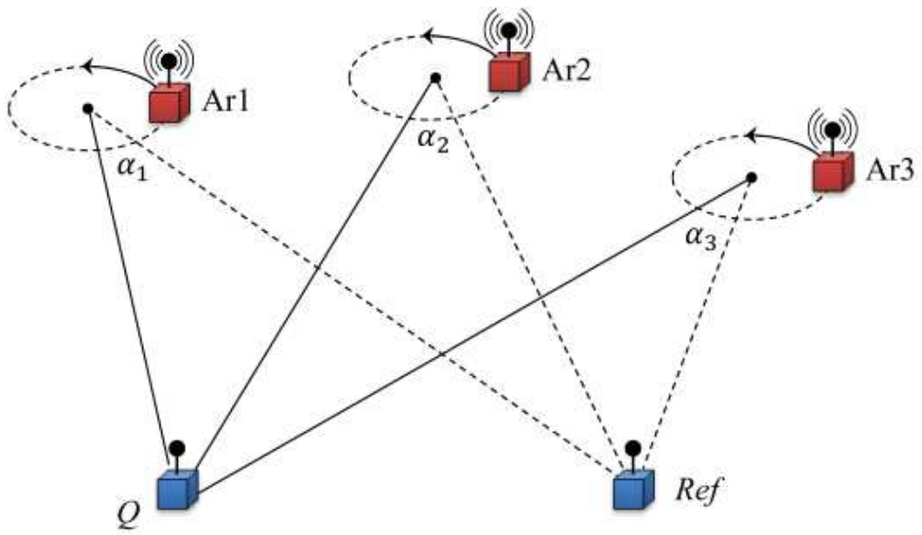

Fig. 11. Localization based on bearing estimates towards rotating transmitter nodes.

SpinLoc experimental measurements in an 8×10 m indoor garage area showed an average bearing estimation accuracy of 3° leading to a localization accuracy of approximately 40 cm. The data collection time is reported by Chang et al. (2008) to be less than 1.5 s, while the per target node localization to be approximately 0.5 s.

The quasi-Doppler localization system proposed in Sallai et al. (2009) generates the interference signal with two anchor nodes. One of these anchor nodes switch the continuous, unmodulated carrier between the antennas of the array. A third anchor node and a target node act as receiver and measure the phase jumps caused by the virtual re-location of the transmitter antenna and reconstruct the quasi Doppler-shift of the signal. The Doppler-shift estimates are then sent to the a PC to estimate the bearings and calculate the target node position. Sallai et al. (2009) present experiments that verify the feasibility of the approach, but no thorough evaluation of the expected accuracy is available.

5. Radio interferometric bearing estimation

The first techniques for bearing estimation in WSNs relied both on radio interferometry and a secondary phenomenon, the Doppler-effect. While these techniques provided bearing estimates of adequate precision for node localization and significantly simplified the sensor fusion algorithm, they called for specialized hardware on a subset of the WSN nodes. To mitigate this unwelcome requirement, Amundson et al. (2010) presents another approach that uses the same uniform, simple WSN nodes as the original RIPS discussed in Section 2, yet it is capable of accurately estimating the bearing from anchor nodes. Note, however, that even though specialized hardware is not required, the method assumes a specific arrangement of certain nodes.

The baseline approach of the method presented in Amundson et al. (2010) is to group together three of the four nodes participating in a typical radio interferometric measurement described in 2. The three nodes, two transmitters and a receiver, placed together in a known and fixed geometry, form a composite anchor node. During the interferometric measurement, the

estimated phase difference between the receiver of the composite anchor node and the target node constraints the location of the latter to a hyperbola. The bearing of the target node to the anchor node is estimated by the asymptote of the hyperbola.

The rest of the section details the theoretical background of the bearing estimation approach, the prototype system used for experimental measurements and the reported results.

5.1 Bearing estimation using 3-node anchors

The bearing estimation phase starts with a regular interferometric measurement where the location of three closely placed nodes is known a priori. These three nodes, M, A_1 and A_2, form a composite anchor from which a receiver node, R, with unknown location estimates its bearing, see Figure 12 (a). Two nodes of the anchor, A_1 and M, transmit unmodulated sinusoid signals at close frequencies, generating an interference signal with a low-frequency envelope. The receiver nodes, A_2 and R measure the phase of the envelope signal according to Equation 9. The measured $\vartheta_{MA_1A_2R} = \vartheta_R - \vartheta_{A_2}$ phase difference is related to the linear combination of the distances between the transmitters according to Equation 15. Thus,

$$\vartheta_{MA_1A_2R} = 2\pi \frac{d_{MR} - d_{A_1R} + d_{A_1A_2} - d_{MA_2}}{c/f} \pmod{2\pi}, \tag{38}$$

where $\lambda = c/f$ is the wavelength of the carrier signal and d is the distance between the nodes denoted in the index. Assuming that the pairwise distance between the three nodes in the anchor is the same, $d_{A_1A_2} - d_{MA_2} = 0$, the expression of the q-range gets simpler, and Equation 38 becomes

$$\vartheta_{MA_1A_2R} = 2\pi \frac{d_{MR} - d_{A_1R}}{c/f} \pmod{2\pi}. \tag{39}$$

The distance difference $d_{MR} - d_{A_1R}$ is of high importance, thus it is shortened as d_{A_1MR}, and referred to as *t-range*. The d_{A_1MR} t-range takes its maximum when R is colinear with the two transmitters A_1 and M. According to Equation 39 the measured distance difference is 2π-ambiguous if the distance between the two transmitters is larger than $\lambda/2$. Thus, with the assumption that the antennas of the anchor nodes are less than half wavelength apart, the modulo 2π is removed and t-range is simplified to

$$d_{A_1MR} = \frac{\vartheta_{MA_1A_2R}}{2\pi} \cdot \lambda. \tag{40}$$

According to Equation 40, the distances between the receiver node and the two transmitter nodes have a constant difference. Thus, d_{A_1MR} in Equation 40 defines the arm of a hyperbola that intersects with the position of node R as shown in Figure 12 (b).

The possible location coordinates (x, y) of R can be expressed with the general equation of the origin centered hyperbola:

$$\frac{x^2}{a^2} - \frac{y^2}{b^2} = 1. \tag{41}$$

Assuming $d_{A_1R}, d_{MR} \ll d_{A_1M}$, the bearing of the R can estimated with the asymptote of the hyperbola. The bearing α of R relative to the origin can then be written using the two

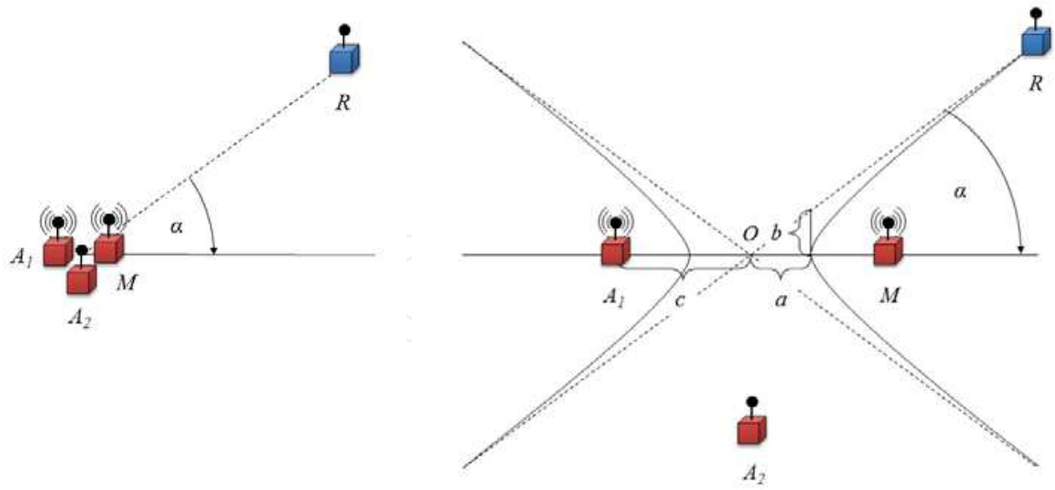

(a) Relative bearing from the 3-node anchor

(b) The 3-node anchor exaggerated to show distances

Fig. 12. Bearing estimation using 3-node anchors

parameters of the hyperbola, a and b:

$$\alpha = \tan^{-1}\left(\frac{b}{a}\right). \tag{42}$$

To find the value of a and b consider the point where the hyperbola arm intersects the line connecting the two focus points. As the distance differences between the foci and *all* points of the hyperbola are the same constant, this point is no exception. Therefore, denoting the distance between the origin and the foci as c and using the t-range definition:

$$d_{A_1R} - d_{MR} = (c + a) - (c - a) = 2a, \tag{43}$$

where c is also known as the linear eccentricity of the hyperbola, for which $c = \sqrt{a^2 + b^2}$ and $c = d_{A_1M}$. Thus, $b = \sqrt{c^2 - a^2}$ and in terms of distances, the value of a and b and the bearing estimate becomes

$$a = (d_{A_1R} - d_{MR})/2 \tag{44}$$

$$b = \sqrt{(d_{A_1M}/2)^2 - ((d_{A_1R} - d_{MR})/2)^2} \tag{45}$$

$$\alpha = \tan^{-1}\left(\frac{\sqrt{(d_{A_1M}/2)^2 - ((d_{A_1R} - d_{MR})/2)^2}}{(d_{A_1R} - d_{MR})/2}\right). \tag{46}$$

The bearing estimate α is, however, ambiguous. First, the hyperbola has two arms. The sign of $d_{A_1R} - d_{MR}$, and thus the sign of the phase difference $\vartheta_R - \vartheta_{A_2}$ selects the arm of the hyperbola. In case $\vartheta_R < \vartheta_{A_2}$, R lies on the left arm, otherwise it lies on the right arm. Second, the $\pm\alpha$ values, relative to the transverse axis of the hyperbola, are both solutions of Equation 46. A second measurement with swapped anchor node roles is used to resolve this

ambiguity. Node A_1 and A_2 switch transmitter-receiver roles at the anchor, defining a new transverse axis and $\pm\alpha$ values relative to it. When the $\pm\alpha$ values from the two measurements are compared to the same reference orientation, two of them coincide, yielding the final bearing estimate. Once the bearing estimates are available from a target node to a set of anchor nodes, simple triangulation can be used for localization.

5.2 Platform description and results

The first experimental implementation of the radio interferometry based bearing estimation was named TripLoc presented in Amundson et al. (2010). The nodes in TripLoc are equipped with fine tunable CC1000 radio chips operating in the 433 MHz band and processing it with a microcontroller at a 9 kHz rate.

The basic TripLoc measurement is a series of radio interferometric phase measurements with four participants, three of which form an anchor node with a priori known location. The measurement starts with two nodes of the anchor transmitting unmodulated carriers at close frequencies. The third node of the anchor and another node with unknown location then synchronize their clocks and measure the phase of the envelope signal. The phase measured by the anchor-receiver is transmitted to the receiver to be localized, which in turn calculates the phase offset. The same measurement is then repeated with the anchor-receiver switching role with one of the transmitters. Using the two phase offsets the receiver node is able to calculate its t-range, see Equation 40, and estimate its bearing to the anchor node according to Equation 46. After repeating the bearing estimation relative to another anchor node, TripLoc uses triangulation to determine the non-anchor receiver node location. As the non-anchor node always acts as a "passive receiver", multiple receivers can participate in the same measurement and calculate their own location simultaneously.

TripLoc experiments using a 16-node setup on a 20×20 m low-multipath environment, with four anchor nodes at the corners, showed that receiver nodes are capable of bearing estimation with an average error of approximately 3°. After triangulation, the average overall position error was 78 cm, while the whole localization took less then 1 second.

6. Stochastic radio interferometric positioning

The localization algorithms presented in Sections 2, 4 and 5 are all based on radio interferometry, where two independent transmitter nodes generate an interference signal by transmitting unmodulated carriers at close frequencies. The radio interferometric localization discussed in Section 2 and the radio interferometric bearing estimation in Section 5 measure the phase of this interference signal, while the Doppler-shift based bearing the frequency of that. However, regardless of the way this interference signals is processed at further stages, all of these methods assume that the interference signal has a low frequency. The fine grained control over the transmit frequencies available on the 433 MHz/950 MHz ISM band CC1000 radio chip based platforms is not present on the increasingly popular 2.4 GHz radio chips, which renders this assumption invalid. The recently presented radio interferometric localization method introduced in Dil & Havinga (2011), therefore, drops this assumption and places most of its processing steps on stochastic bases. The rest of the section presents the theory behind the stochastic radio interferometric positioning by highlighting the key

differences with the original "deterministic" approach, shows a 2.4 GHz band CC2430 radio chip based implementation and the corresponding localization experimentation results.

6.1 Stochastic interferometric localization

Similarly to the original radio interferometric positioning method, the stochastic approach starts with two nodes transmitting unmodulated carriers at close frequencies. As fine-grained control over the transmit frequencies is not assumed, the calibration phase is omitted as shown in Figure 13. As a result, the frequency value of the two transmitted signals becomes unknown and the difference of the two has a significantly higher variance than in case of the original method after calibration. The high variance of the interference frequency, in turn, manifests in numerous measurements with interference frequency too low or too high for precise phase estimation. This ultimately generates a significantly higher number of inaccurate phase measurements, hence, the phase estimate is treated by the upcoming stochastic processing stages as a random variable. Despite the fact that a significant number of the phase measurements are likely to be corrupted, the phase measurement process is identical to that of the one presented in Section 2. That is, with carrier frequencies f_A and f_B of transmitters A and B, where $f_A > f_B$ is assumed:

$$\Delta\varphi_i = 2\pi \left(\frac{d_{AD} - d_{AC}}{\lambda_A} - \frac{d_{BD} - d_{BC}}{\lambda_B} \right) \mod (2\pi) \tag{47}$$

$$\approx 2\pi \left(\frac{d_{ABCD}}{\lambda_i} \right) \mod (2\pi), \tag{48}$$

where $\Delta\varphi_i$ is, again, the relative phase offset of the envelope frequencies at the two receivers, d_{XY} is the distance of the corresponding nodes X and Y, and λ_i is defined as $\lambda_i = 2c/(f_A + f_B)$.

Again, Equation 48 provides the q-range value with a 2π ambiguity, which is removed in the method in Section 2 by repeating the same measurement over a set of different carrier frequencies to obtain the q-range. The stochastic method takes a different approach here, as shown in Figure 13. Rather than calculating the q-range error distribution first, then estimating the q-range values and then the node positions, it calculates only the q-range error distributions and uses them to estimate the positions directly:

$$(\hat{x}, \hat{y}) = \arg\min_{\hat{x},\hat{y}} \sum_{j=1}^{M} \sum_{i=1}^{N} \left(\Delta\varphi_{i,j} - \Delta\hat{\varphi}_{i,j} \right)^2 \tag{49}$$

$$= \arg\min_{\hat{x},\hat{y}} \sum_{j=1}^{M} \sum_{i=1}^{N} \left(d_{i,j} - \hat{\mathrm{q}}_j \right)^2 \tag{50}$$

$$= \arg\min_{\hat{x},\hat{y}} \sum_{j=1}^{M} \mathrm{error}(\hat{\mathrm{q}}_j) \tag{51}$$

That is, the stochastic method minimizes Equation 51, where $\Delta\hat{\varphi}_{i,j}$ is the estimated phase offset calculated by the location estimate, $d_{i,j}$ is defined by Equation 17, $\hat{q}_j$ is the q-range estimate and error$(\hat{q}_j)$ is the q-range error distribution. As the latter one oscillates rapidly, it is not

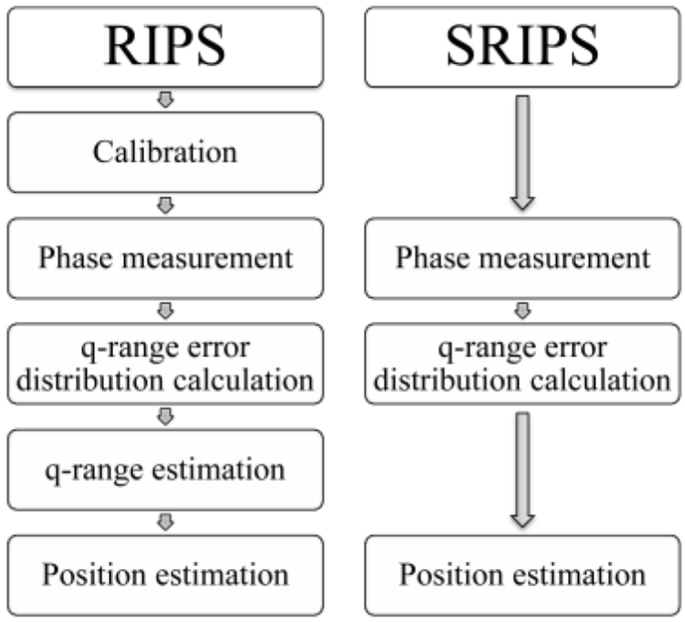

Fig. 13. Comparison of the original (RIPS) and the stochastic interferometric localization algorithms

minimized directly. Rather, it is smoothed first by taking its envelope and then, the minimum of the envelope is searched.

6.2 Platform description and results

The key motivation behind the Stochastic Radio Interferometric Positioning System (SRIPS), detailed in Dil & Havinga (2011), was to make inteferometric localization available on WSN platforms using radio chips operating in the 2.4 GHz band. Popular 2.4 GHz radio chips, such as the CC2430 Texas Instruments (2007b), offer no mechanism to fine tune the transmit frequency. However, they support much higher sampling rates than the CC1000 radio. As a result, the synthesized interference signal envelope frequency has a larger variance, with high confidence in the 200 Hz to 14 kHz range, but it is sampled at a rate of 62.5 kHz.

The SRIPS phase measurement starts with two nodes transmitting unmodulated carriers at nominally same frequencies – without making attempts to fine tuning. The receiver nodes measure the envelope phase and transmit it to a PC. The same phase measurement is carried out over a set of frequencies and is repeated for different transmitter pair combinations. Due to the inaccurately set interference signals, several of the phase measurements are invalid. To cope with the large number of inaccurate measurements, SRIPS skips the q-range calculation step and optimizes Equation 51 on the PC using the phase offsets directly.

SRIPS experiments on a 20×20 m field resulted in an average error of 50 cm.

7. Summary

The algorithms presented in this chapter all rely on radio interferometry in order to localize or track nodes in WSNs. In each case, the interference signal is generated the same way,

by two independent transmitters, but the different algorithms exploit features of this signal in different ways. Table 2 compares the algorithms with an emphasis on the experimental implementation and key results. All the prototype systems expect for SRIPS rely on the CC1000 radio chipset, which is designed operate in the 433 MHz and 900 MHz bands. They are characterized by a precisely tuned interference frequency which allows for processing at the limited 9 kHz sampling rate. Clearly, it is the unique fine-tuning capability of the CC1000 LO that made this radio chip - along with the MICA2 platform - the most favorable choice. SRIPS, on the other hand, aimed to make interferometric localization available on platforms that lack a fine-tunable LO. Driven by the reduced control over the interference frequency in the CC2430, SRIPS decided to drop tuning altogether. The available higher 62.5 kHz sampling rate made the processing of the highly varying frequency interference signal possible. This came at the cost of significantly increased number of inaccurate phase measurements, which SRIPS deals with in later processing stages.

	RIPS	SRIPS	RIPS bearing	Doppler tracking	Doppler bearing
Radio chip	CC1000	CC2430	CC1000	CC1000	CC1000
Operating band	433 MHz	2400 MHz	433 MHz	433 MHz	900 MHz
Sampling frequency	9 kHz	62.5 kHz	9 kHz	9 kHz	9 kHz
Interference frequency	300-700 Hz	200-12000 Hz	300-700 Hz	300-700 Hz	300-700 Hz
Special hardware required	No	No	No	No	Yes
Anchor nodes required	No	No	Yes	Yes	Yes
Localization time	Several minutes	Several minutes	Few seconds	Few seconds	Few seconds
Average error	< 5 cm	50 cm	80 cm	1.5 m	40 cm

Table 2. Comparison of RI localization systems

An important aspect in several applications is whether the localization or tracking service requires additional hardware. RIPS, SRIPS, RIPS bearing and Doppler tracking are especially favorable as they rely on no extra hardware. RIPS bearing, however, uses a special arrangement of certain nodes, which might be unfavorable in certain scenarios. Doppler bearing approaches utilize either a physically rotating antenna, or a relatively complex antenna array—both of which are impractical in low-cost WSNs.

RIPS and SRIPS are unique in the sense that they are able to calculate the relative node locations without anchor nodes, that is, without prior knowledge of locations of a subset of nodes. In this mode, they generally require orders of magnitude more time to do the self-localization. The presence of anchor nodes may potentially speed up the localization process both for RIPS and SRIPS, while it is essential for the other systems. In general,

RIPS bearing, Doppler tracking and Doppler bearing leverage the prior knowledge of the anchor node locations and allow for distributed calculation of the locations, e.g. the nodes can estimate their own positions.

The operating range of the presented radio interferometric platforms is generally in the order of tens of meters up to a few hundred meters. In multipath free environments, the original RIPS proves to be the most accurate, which is, again, mainly due to the favorable properties of the CC1000. This is followed by the Doppler bearing, SRIPS and RIPS bearing, each of which achieves sub-meter accuracy. The average error of Doppler tracking is difficult to compare as it assumes the initial positions to be known and because the error is calculated over several iterations.

8. Nomenclature

Anchor node	Node with a priori known location
COTS	Commercial Off-The Shelf
IF	Intermediate Frequency
LO	Local Oscillator
PC	Personal Computer
RIPS	Radio Interferometric Positioning System
RSS	Received Signal Strength
SRIPS	Stochastic Radio Interferometric Positioning System
WSN	Wireless Sensor Network

Table 3. List of acronyms

9. References

Amundson, I., Sallai, J., Koutsoukos, X. & Lédeczi, A. (2010). Radio Interferometric Angle of Arrival Estimation, *7th European Conference on Wireless Sensor Networks*, Springer, Coimbra, Portugal.
URL: *http://www.isis.vanderbilt.edu/node/4139*

Chang, H.-l., Tian, J.-b., Lai, T.-T., Chu, H.-H. & Huang, P. (2008). *Spinning beacons for precise indoor localization*, ACM Press, New York, New York, USA.
URL: *http://portal.acm.org/citation.cfm?id=1460412.1460426*

Dil, B. J. & Havinga, P. J. M. (2011). Stochastic Radio Interferometric Positioning in the 2.4 GHz Range, *Proceedings of the 9th ACM conference on Embedded network sensor systems - SenSys'11*, ACM Press, Seattle, WA, USA.

Fontana, R. J., Richley, E. & Barney, J. (2003). Commercialization of an ultra wideband precision asset location system, *IEEE Conference on Ultra Wideband Systems and Technologies 2003*, number November, IEEE, IEEE, pp. 369–373.
URL: *http://ieeexplore.ieee.org/lpdocs/epic03/wrapper.htm?arnumber=1267866*

Kusý, B., Balogh, G., Völgyesi, P., Sallai, J., Nádas, A., Maróti, M., Meertens, L. & Lédeczi, A. (2006). Node-density independent localization, *Information Processing in Sensor Networks (IPSN 06) SPOTS Track*.

Kusý, B., Lédeczi, A. & Koutsoukos, X. (2007). *Tracking mobile nodes using RF Doppler shifts*, ACM Press, New York, New York, USA.
URL: *http://portal.acm.org/citation.cfm?id=1322263.1322267*

Lédeczi, A., Völgyesi, P., Sallai, J. & Thibodeaux, R. (2008). *A novel RF ranging method*, IEEE. URL: *http://ieeexplore.ieee.org/xpl/freeabs_all.jsp?arnumber=4623303*

Maróti, M., Völgyesi, P., Dóra, S., Kusý, B., Nádas, A., Lédeczi, A., Balogh, G. & Molnár, K. (2005). *Radio interferometric geolocation*, ACM Press, New York, New York, USA. URL: *http://portal.acm.org/citation.cfm?id=1098918.1098920*

Sallai, J., Völgyesi, P. & Lédeczi, A. (2009). Radio interferometric Quasi Doppler bearing estimation, *IPSN '09 Proceedings of the 2009 International Conference on Information Processing in Sensor Networks*, IEEE Computer Society, Washington, DC, USA, pp. 325–336. URL: *http://portal.acm.org/citation.cfm?id=1602165.1602195*

Taubenheim, D., Kyperountas, S. & Correal, N. (2005). Distributed radiolocation hardware core for ieee 802.15.4, *Technical report*, Motorola Labs, Plantation, Florida.

Texas Instruments (2007a). Single-chip very low power RF transceiver, *Technical report*, Texas Instruments. URL: *http://www.ti.com/lit/ds/symlink/cc1000.pdf*

Texas Instruments (2007b). A true system-on-chip solution for 2.4 GHz IEEE 802.15.4 / zigbee(tm), *Technical report*, Texas Instruments. URL: *http://www.ti.com/lit/ds/symlink/cc2430.pdf*

Tuchler, M., Schwarz, V. & Huber, A. (2005). Location accuracy of an UWB localization system in a multi-path environment, *2005 IEEE International Conference on UltraWideband* (September): 414–419. URL: *http://ieeexplore.ieee.org/lpdocs/epic03/wrapper.htm?arnumber=1570023*

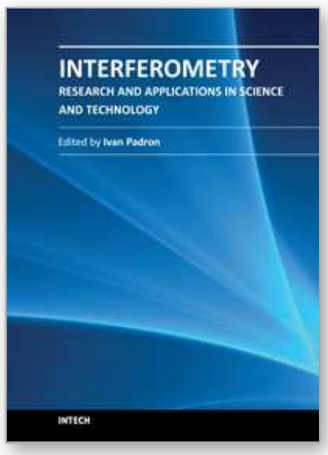

Interferometry - Research and Applications in Science and Technology

Edited by Dr Ivan Padron

ISBN 978-953-51-0403-2
Hard cover, 462 pages
Publisher InTech
Published online 21, March, 2012
Published in print edition March, 2012

This book provides the most recent studies on interferometry and its applications in science and technology. It is an outline of theoretical and experimental aspects of interferometry and their applications. The book is divided in two sections. The first one is an overview of different interferometry techniques and their general applications, while the second section is devoted to more specific interferometry applications comprising from interferometry for magnetic fusion plasmas to interferometry in wireless networks. The book is an excellent reference of current interferometry applications in science and technology. It offers the opportunity to increase our knowledge about interferometry and encourage researchers in development of new applications.

InTech Europe
University Campus STeP Ri
Slavka Krautzeka 83/A
51000 Rijeka, Croatia
Phone: +385 (51) 770 447
Fax: +385 (51) 686 166
www.intechopen.com

InTech China
Unit 405, Office Block, Hotel Equatorial Shanghai
No.65, Yan An Road (West), Shanghai, 200040, China
中国上海市延安西路65号上海国际贵都大饭店办公楼405单元
Phone: +86-21-62489820
Fax: +86-21-62489821

IntechOpen